Journal of
Applied Remote Sensing

Ground demonstration of trace gas lidar based on optical parametric amplifier

Kenji Numata
Haris Riris
Steve Li
Stewart Wu
Stephan R. Kawa
Michael Krainak
James Abshire

Ground demonstration of trace gas lidar based on optical parametric amplifier

Kenji Numata,[a,b] Haris Riris,[b] Steve Li,[b] Stewart Wu,[b] Stephan R. Kawa,[b] Michael Krainak,[b] and James Abshire[b]

[a]University of Maryland, Department of Astronomy, College Park, Maryland 20742
kenji.numata@nasa.gov
[b]NASA Goddard Space Flight Center, Greenbelt, Maryland 20771

Abstract. We report on the development effort of a nanosecond-pulsed optical parametric amplifier (OPA) for remote trace gas measurements for Mars and Earth. The OPA output has ~500 MHz linewidth and is widely tunable at both near-infrared and mid-infrared wavelengths, with an optical—optical conversion efficiency of up to ~39%. Using this laser source, we demonstrated open-path measurements of CH_4 (3291 and 1652 nm), CO_2 (1573 nm), H_2O (1652 nm), and CO (4764 nm) on the ground. The simplicity, tunability, and power scalability of the OPA make it a strong candidate for general planetary lidar instruments, which will offer important information on the origins of the planet's geology, atmosphere, and potential for biology. [DOI: 10.1117/1.JRS.6.063561]

Keywords: optical parametric amplifier; lidar; differential absorption lidar; space instrumentation.

Paper 12059P received Mar. 8, 2012; revised manuscript received Jun. 17, 2012; accepted for publication Jul. 19, 2012; published online Sep. 12, 2012.

1 Introduction

Laser remote-sensing measurements of trace gases from orbit can provide unprecedented information about important planetary science and answers to critical questions regarding planetary atmospheres. Carbon dioxide (CO_2), methane (CH_4), and carbon monoxide (CO) are three very important greenhouse gases on Earth. Remote sensing of these gases will assist in understanding Earth's climate change and will help to reduce the uncertainty in the carbon budget. NASA's decadal survey[1] called for a mission to measure CO_2, CH_4, and CO. Remote measurements of CH_4, water (H_2O), and other biogenic molecules (such as ethane and formaldehyde) on Mars have important connections to questions related to the existence of life on Mars.[2] Localized areas with higher gas concentrations could become a primary target of future landing missions. Our aim is to increase the accuracy of mapping of these gases globally through integrated path differential absorption (IPDA) lidar measurements with much higher accuracies by developing a near-infrared (NIR) and mid-infrared (MIR) lidar transmitter. Most trace gases on Mars and Earth have suitable spectral absorption features in the NIR ($1.5 \sim 1.6\ \mu$m) and MIR ($3 \sim 5\ \mu$m) regions. Our tunable laser transmitter and high-sensitivity detectors at NIR and/or MIR when used in a sounding (surface reflection) mode enable IPDA measurements from orbit with modest laser power.

At NASA Goddard Space Flight Center (GSFC), we are developing a laser transmitter system for both Mars and Earth applications. Our system is based on a nanosecond-pulsed optical parametric amplifier (OPA) pumped at 1064 nm with magnesium oxide—doped periodically poled lithium niobate (MgO:PPLN) as the nonlinear medium. The OPA is suited for this application since it has a sufficient wavelength tuning range for gas detection and it generates both NIR and MIR, whereas traditional tunable lasers, such as external cavity diode lasers or quantum cascade lasers, do not generally have sufficient pulse energy (~few 100 μJ) for space-borne measurements. The two outputs at NIR and MIR are called "signal" and "idler," respectively. The output wavelengths of signal and idler can be tuned by adjusting a seed laser in the OPA. While our

0091-3286/2012/$25.00 © 2012 SPIE

primary target is CH_4 on Earth and Mars, the OPA approach will add a new capability for general planetary lidar instruments. In parallel, we continue to examine narrower-band sources such as Yb fiber amplifier pumped optical parametric oscillator (OPO) and stand-alone Er:YAG lasers. These may ultimately achieve higher wall-plug efficiency.[3,4] However, the OPA clearly provides a convenient light source for the measurement of numerous gases.

Although many gas sensing lidar systems are based on OPO approaches,[5–11] our OPA approach is simpler, especially when narrow-linewidth, high-power pump and seed lasers are available. Owing to the optical feedback provided by the resonant cavity, an OPO generally offers higher output beam quality, narrower output linewidth, and higher electrical-to-optical efficiency. However, it is sensitive to alignment, does not allow easy continuous tuning, and requires more optics, electronics, and frequent adjustment. High nonlinearity of a quasi-phase matched device (such as PPLN) allows efficient generation of NIR and MIR energy even with the single-pass OPA configuration. We think the simplicity and robustness of the OPA's optical arrangement make it a strong candidate for space applications, particularly Earth remote sensing. This type of single-pass device previously required high pump peak power with picosecond pulsewidths. However, nanosecond pulsewidths are required for gas-sensing applications to obtain the narrower transform-limited linewidths needed to resolve target gas lines. This type of nanosecond OPA system based on PPLN was previously primarily constructed with Nd:YAG microchip pump lasers.[12–15]

In this paper, we report on the setup of the developed OPA system and measurements of diurnal variation of Earth's atmospheric CH_4, CO_2, H_2O, and CO using horizontal absorption paths.

2 Experimental Setup

2.1 *Overview*

We have built three OPA systems, designated as OPA system 1. OPA system 2. and OPA system 3. in this paper. Figure 1 shows the experimental diagram of OPA system 1. In this system, both signal (1573 nm) and idler (3291 nm) are used for the simultaneous measurements of CH_4 and

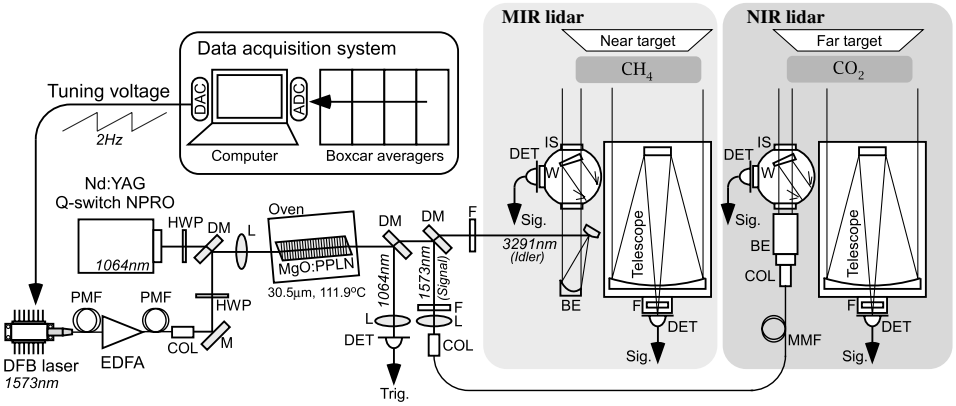

Fig. 1 Experimental diagram. A MgO:PPLN crystal is pumped and seeded by a Q-switch Nd:YAG NPRO and a DFB laser, respectively. In OPA system 1 (1573-nm seed), both signal and idler are used for lidar measurement as shown in this figure. In OPA system 2 (1651-nm seed), only the signal is used for lidar measurement and there is no EDFA and MIR lidar. In OPA system 3 (1371-nm seed), only the idler is used for lidar measurement and there is no EDFA and NIR lidar. EDFA: Erbium-doped fiber amplifier, HWP: half wave-plate, M: mirror, DM: dichroic mirror, L: lens, F: wavelength-selecting filter, COL: fiber collimator, IS: integrating sphere, W: wedge, DET: detector, BE: beam expander, PMF: single-mode polarization maintaining fiber, MMF: multi-mode fiber, ADC: analog-to-digital converter, DAC: digital-to-analog converter, Trig.: trigger signal for boxcar averagers, Sig.: Signal input for boxcar averager.

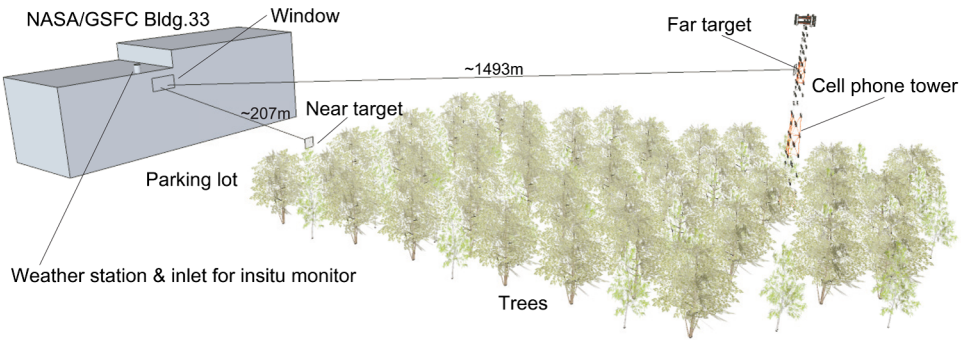

Fig. 2 Schematic view of two open paths. The MIR lidars (idlers of OPA systems 1 and 3) used the near target. The NIR lidars (signals of OPA systems 1 and 2) used the far target.

CO_2 using the near and far targets (as shown in Fig. 2), respectively. A nonlinear crystal is pumped by a pulsed 1064 nm Nd:YAG laser and seeded by a continuous-wave distributed-feedback (DFB) laser diode (LD) through an Erbium-doped fiber amplifier (EDFA). OPA system 2 has a similar setup, except that only the signal wavelength near 1651 nm is used for CH_4 and H_2O measurements using the far target. OPA system 3 is implemented upon OPA system 1 by swapping the nonlinear crystal and the seed laser. Its idler at 4764.0 nm is used for the measurement of CO. No fiber amplifier is employed for the seed in OPA systems 2 and 3, since no fiber amplifier works at their seed wavelengths. Table 1 summarizes the specifications for the three OPA lidar systems.

2.2 *OPA Source*

The pump source is a passively Q-switched Nd:YAG nonplanar ring oscillator (NPRO) made by Innolight Inc. that emits single-frequency, single longitudinal-mode output at 1064.5 nm. It has ~3.3-ns pulse width and ~60-μJ pulse energy at a ~6-kHz repetition rate. The optical linewidth of the NPRO is transform limited (~133 MHz).

The seed source is a continuous-wave, PM (polarization-maintaining) fiber-coupled, DFB LD. The instantaneous linewidth of DFB LD is less than 1 MHz. The wavelengths of the DFB LDs are selected to be 1573.3, 1651, and 1370.8 nm for OPA systems 1, 2, and 3, respectively. The 1573.3-nm LD is FRL15DCWD from Furukawa Electric, Japan. The 1651- and 1370.8-nm LDs are NLK series from NTT Electronics, Japan. The 1651-nm LD for OPA system 2 is step-scanned between 1650.9 and 1652.0 nm for CH_4 and H_2O measurements, respectively, by applying a step temperature change of 7.2°C with an interval of 5 min. The DFB LD can be smoothly tuned through a wide range (>0.25 nm or ~30 GHz) without a mode hop, by injection current modulation. As a result, the output idler and signal can be tuned without a mode hop across the absorption peaks of the target gases. The seed LDs are tuned by a ramp voltage at 2 Hz. We observed that use of a higher-seed optical power ensures smooth tuning as well as high efficiency. When the seed has low power and a slight misalignment, the signal was obscured by the amplified vacuum fluctuation and/or a parasitic parametric oscillation. Therefore, we used a minimum seed power of ~15 mW (for OPA systems 2 and 3). For OPA system 1 at 1573.3 nm, we amplified the seed to ~300 mW using a PM EDFA.

The seed beam is co-aligned with the pump using a dichroic mirror. The beams are focused down to a crystal by a lens with a focal length of 300 mm. The resultant beam radii inside the crystal are ~100 and ~125 μm for the pump and the seed, respectively. The locations of the beam waists are carefully adjusted to overlap with each other. With this pump beam size, the crystal is operated near the threshold of optical parametric generation (OPG).

The nonlinear crystal is a 50-mm-long, 1-mm-thick MgO:PPLN. The end surfaces of the crystal were angled at 5 deg and anti-reflective (AR) coated at the pump, the signal, and the idler wavelengths to minimize optical feedback. A similar angle-cut crystal arrangement can be found, for example, in Ref. 16. We observed that the output signal/idler wavelengths do not smoothly follow the scanned seed if the end surfaces of the crystal are not angled. This

Table 1 Technical data for the three OPA lidar systems.

	OPA system 1		OPA system 2		OPA system 3
Target gas (wavelength)	CH_4 (3291.1 nm)	CO_2 (1573.3 nm)	CH_4 (1650.9 nm)	H_2O (1652.0 nm)	CO (4764.0 nm)
Pumping					
Pump source	LD-pumped, passively Q-switched, Nd:YAG NPRO				
Pump pulse width	~3.3 nsec				
Incident pump energy	~60 μJ				
Repetition rate	~6 kHz				
OPA					
Nonlinear medium	MgO:PPLN, 50 $(L) \times 8$ $(W) \times 1$ mm (H), 5-deg angle cut, AR coated				
Grating period	30.5 μm		31.0 μm		26.4 μm
Temperature	111.9°C		128.4°C		109.5°C
Beam radius	~100 μm for pump, ~125 μm for seed				
Output pulse width	~2 ns				
Output energy	~7.6 μJ	~16 μJ	~13 μJ		~1.9 μJ
Output linewidth	~500 MHz				~700 MHz
Seeding					
Seed laser	Telecom DFB LD, PM fiber coupled				
Wavelength	1573.3 nm		1650.9/1652.0 nm (temperature tuned)		1370.8 nm
Amplifier	PM EDFA		Not used		Not used
Seed power	~300 mW		~15 mW		~15 mW
Scan	2 Hz, ramped, current tuning				
Transmitter					
Integrated sphere coating	Infragold	Spectralon	Spectralon		Infragold
Beam expander	Reflective	Refractive	Refractive		Reflective
Wedge material	CaF_2	BK7	BK7		CaF_2
Receiver					
Telescope	200-mm diameter, Cassegrain				
Detector	HgCdTe	InGaAs	InGaAs		HgCdTe

resulted from a parasitic optical parametric oscillation generated by the reflection at the end surfaces. Figure 3 shows the measured tuning curve of the MgO:PPLN crystals. We used a 30.5-μm grating at 111.9°C, 31.0-μm grating at 128.4°C, and 26.4-μm grating at 109.5°C for OPA systems 1, 2, and 3, respectively. The center wavelength of parametric gain at NIR was tuned around 1370, 1575, and 1650 nm, with the three gratings, by tuning the temperature between 70°C and 170°C. The corresponding idler tuning occurred around 4770, 3280, and 3000 nm, respectively. The full-width half-maximum of the unseeded OPG spectra was about 0.3, 1.2, and 2.1 nm at 1370, 1575, and 1650 nm, respectively. As a result, the crystal temperature required no tuning for the two wavelengths (1650.9 and 1652.0 nm) in OPA system

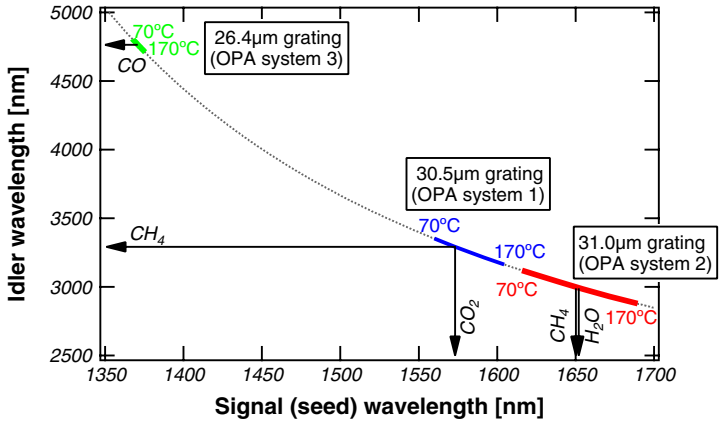

Fig. 3 Tuning curves of the three MgO:PPLN crystals used in the three OPA systems. Wavelengths of the five gas absorption lines used in the lidar measurement are indicated by arrows.

2. Once seeded within the gain bandwidth, the output spectrum collapsed to the seed wavelength with >20-dB suppression.

2.3 *Lidar and Monitor Systems*

The output beam is separated into three paths using dichroic mirrors. The signal at NIR and the idler at MIR are used for gas detection through open paths with cooperative hard targets set at 1493 and 207 m away, respectively, as shown in Fig. 2. The targets are covered by automotive reflective tape. The signal is detected by InGaAs detector with 0.8-mm^2 active area (DET10C from Thorlabs, USA). The idler is detected by HgCdTe detector with 1-mm^2 active area (PVI-5 from VIGO System S.A., Poland). The light goes through a beam expander and a wedge, which is set inside the integrating sphere. The scattered light inside the integrating sphere is detected by the same detector and is used as an energy monitor to normalize the return signals. We have found that this normalization effectively removes instrument fringes. The return beams reflected by the hard targets are received by 20-cm-diameter Cassegrain telescopes with protective aluminum coatings. The pulsed signals from the detectors are averaged by boxcar averagers triggered by the residual pump pulse. Optical cross-talk is avoided by inserting optical filters before the transmitter and after the telescope.

The temperature and pressure values of the atmosphere, which are needed to convert the measured absorption curve into mixing ratios, are monitored by a weather station set at the roof of our building. The weather station also monitors wind speed and wind direction. An in situ cavity ring-down spectrometer by Picarro Inc. monitors CH_4, CO_2, and H_2O mixing ratios of the outside air on the same roof. The lidar systems and the in situ system are set on the fourth floor of one of the buildings at GSFC, in Greenbelt, MD, United States.

3 Experimental Results

3.1 *OPA Characterization*

Figure 4 shows the relationship between pump energies, signal energies, and seed powers in OPA system 1. With a 60-μJ pump and a ~300-mW seed at 1573.3 nm, we obtained a ~16-μJ signal, excluding the effect of ~70% transmittance of wavelength selection filter. The corresponding idler at 3291.1 nm was ~7.6 μJ. Thus, total pump conversion efficiency was $(16\ \mu\text{J} + 7.6\ \mu\text{J})/60\ \mu\text{J} \sim 39\%$.

As shown in Fig. 5(a), the OPA output had a ~2-ns width and a distorted Gaussian pulse shape, which is caused by the back-conversion process between the 1064-nm pump and signal/idler, at full pump energy. At reduced pump energy, the signal output had a shorter width with a near-Gaussian pulse shape. The M^2 of the OPA output signal beam was ~1.3. The output

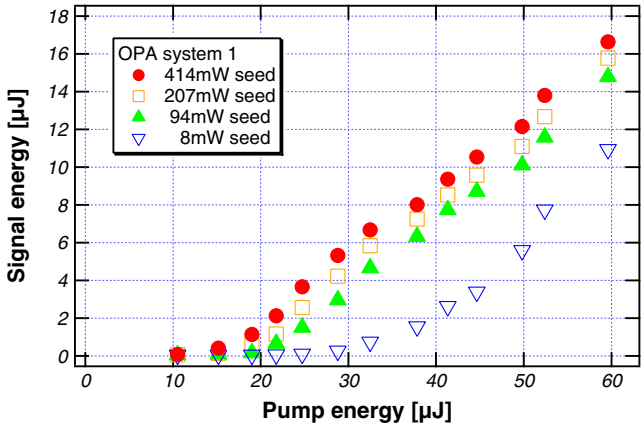

Fig. 4 Relationship between signal and pump energies at different seed-power levels (OPA system 1).

linewidth of the OPA was estimated from both the scanning Fabry-Perot etalon and the gas cells. When the pump energy was low and the crystal was operated near the differential frequency generation (DFG) regime, the linewidth of the signal was measured as near—transform limited (<200 MHz). When the pump energy was high and at our nominal OPA operating condition, the signal was broadened to ~500 MHz (averaged over the beam) due to the back-conversion processes, as shown in Fig. 5(b). In this pump-depleted regime, strong energy exchange occurs among the three frequencies, each of which has finite linewidth, resulting in linewidth broadening. The effect of the broadened linewidth on the measured mixing ratio was small, since the typical pressure-broadened full-width half maximum (FWHM) linewidth of our target line is ~5 GHz. Figure 5(b) and measurements using an optical spectrum analyzer indicated that the side-mode suppression ratio of the OPA output spectrum is >20 dB. Ehret et al.,[17] in their sensitivity analysis for space-borne IPDA lidar for CO_2, CH_4, and N_2O calculated that a spectral purity value of ~99.97% would be required to achieve a 0.022% error in the total optical thickness. Although their definition of the spectral purity differs slightly from the side-mode suppression ratio, we believe that can meet a spectral purity requirement of 99.9% (30 dB) for a 0.1% accuracy space-borne transmitter, by carefully managing the parametric gain and the laser linewidths.

For the same seed power of ~15 mW, the total pump conversion efficiency was ~34%, ~33%, and ~14% for the OPA system 2 (1651-nm seed), 1 (1573-nm seed), and 3 (1371-nm seed), respectively. The higher efficiency for longer-seed wavelengths can be partly attributed to the difference in the parametric gain, which becomes higher at longer-seed wavelengths for the same crystal length and for the same optical power densities.[18] The low efficiency of the OPA

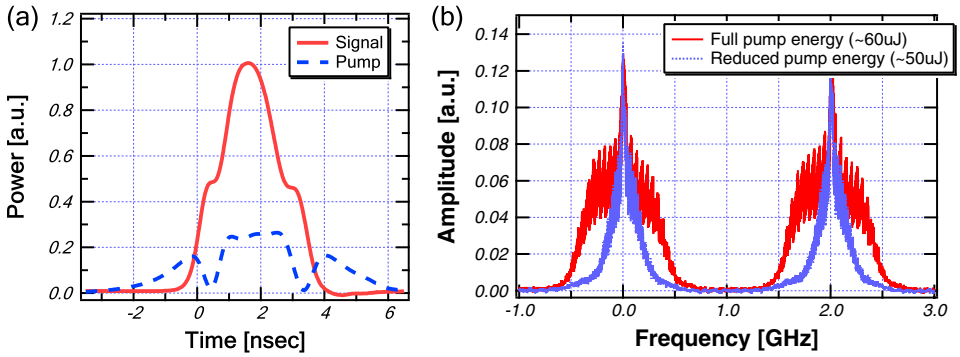

Fig. 5 (a) Typical pulse shapes of the output signal and residual pump (with full pump energy). (b) Typical optical spectrum of the output signal with full and reduced pump energies. This is measured by a scanning Fabry—Perot etalon with 2-GHz free spectral range.

system 3 (26.4-μm grating) was also thought to be a result of the imperfection of the crystal with a shorter grating period.

3.2 *Open Path Scans*

The calculation of the mixing ratio was done by fitting the scan result with theoretical Voigt profile (examples are shown in Fig. 6). To reduce the statistical error, 5 min of the digitized data were averaged. As a result, 10-min interval data of CH_4 and H_2O were alternatively obtained for OPA system 2. The signal from the receiver telescope was divided by the signal from the integrating sphere. The baseline was determined by fitting the divided data, excluding the absorption feature with a fifth-order polynomial function, which removed residual instrumental fringes. The fringes are believed to be from multimode fibers, optical filters, and residual reflections off the crystal surfaces. The CH_4, CO_2, and CO absorptions are affected by the side lobes of nearby H_2O absorption lines and may cause error in the mixing ratio estimation. Therefore, the result from the 1652.0-nm H_2O lidar, which has less contamination from other gas species, was used to correct the baseline of the other lidar data. The data were normalized by both the fitted baseline and the H_2O contribution, and finally fitted to the theoretical Voigt profile[19] using the center wavelength of the scan and a mixing ratio as the fitting parameters. The measured temperature, pressure, and round-trip path lengths were used to calculate the profile. Line parameters (center wavelength, line strength, etc.) are taken from the HITRAN 2008 database.[20] Ten adjacent lines were included into the fitting process.

Figure 7 shows the result of simultaneous measurements of CH_4, CO_2, and H_2O mixing ratio over 50 h (OPA systems 1 and 2). The lidar measurements showed good agreement with in situ data for all three gases. Figure 8 shows the result of independent CO measurement (OPA system 3).

4 Discussion

4.1 *Interpretation of Results*

The agreement between the lidar and the in situ sensor shows that the OPA system is capable of measuring variations in the mixing ratios of the atmospheric gases at both NIR and MIR. Their deviation can be largely explained by the difference between the lidar's column measurement and the in situ device's point measurement. We observed $\sim \pm 0.5$-ppm and $\sim \pm 30$-ppm mixing-ratio variations in CH_4 and CO_2 channels, respectively.

In addition to the weather station data, we obtained meteorological data from the Global Modeling and Assimilation Office (GMAO) at GSFC. The GMAO develops models and assimilates observations from satellites and ground systems to generate meteorological products that

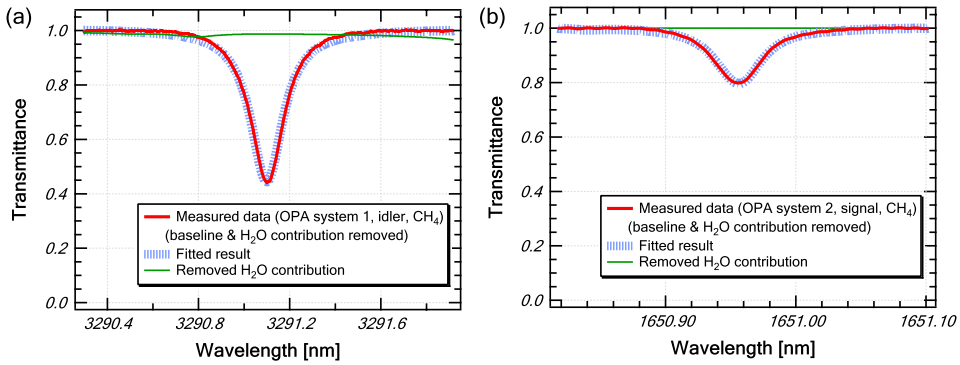

Fig. 6 Examples of measured scan data and fitting results. CH_4 measurement at 3291.1 nm (a) and 1650.9 nm (b) are shown. The scan data were averaged, divided by the signal from the integrating sphere, and further normalized by a polynomial baseline determined from the edge of the data, after the removal of the H_2O contribution.

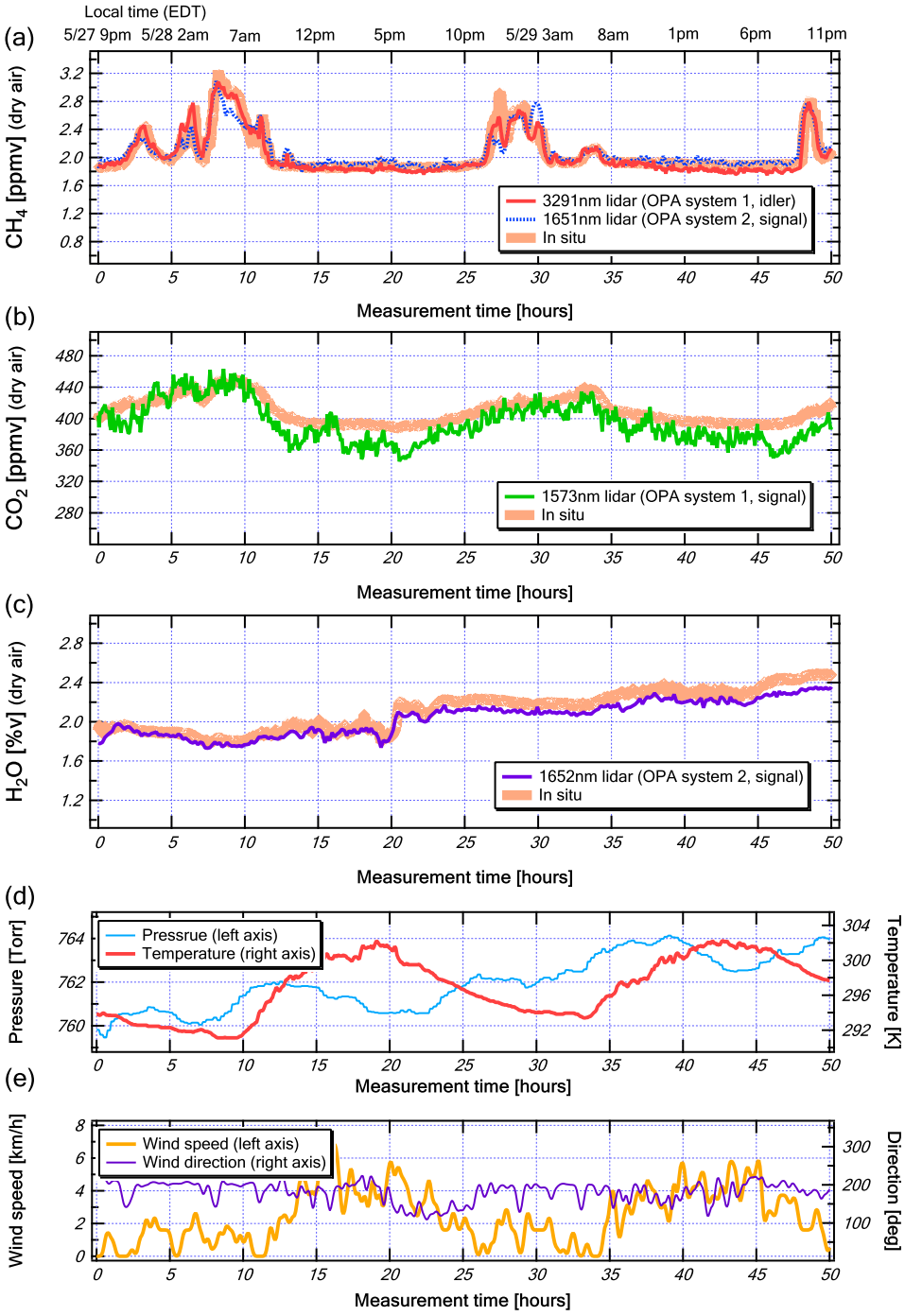

Fig. 7 Simultaneous measurements of the diurnal variations of atmospheric CH_4 (a), CO_2 (b), and H_2O (c) measured with OPA systems 1 and 2, and an in situ sensor. (d) and (e), Meteorological data for the same duration.

are used for a variety of NASA science missions. According to the GMAO analysis, the local boundary-layer height was clearly defined by the potential temperature gradient at about 700 m during daytime of each day. During nighttime, a stable layer was maintained near the surface with little mixing. This and slow wind speed cooperatively allowed the local gas emission to accumulate near the surface at night.

Although it is not clear from the meteorological data, one possible source for the CH_4 enhancements is either a local landfill or the power plant at NASA GSFC, which uses natural

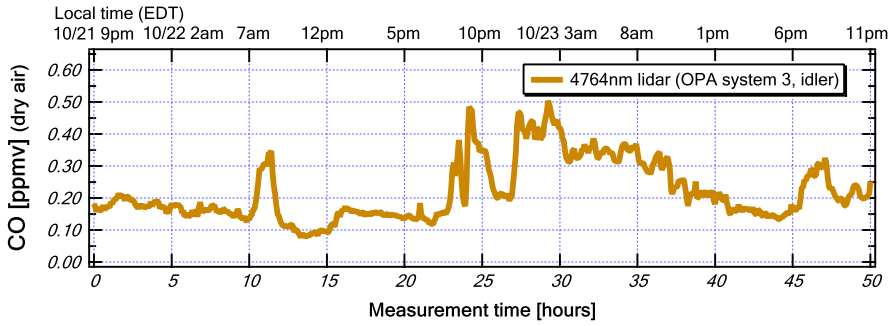

Fig. 8 Measurement of the diurnal variation of atmospheric CO with OPA system 3.

gas from the landfill. This hypothesis is in part supported by the differences observed between the two CH_4 channels. The 3291-nm channel (near target) agrees better with the in situ data, whereas the 1651-nm channel (far target) tended to show slightly different CH_4 variations. This difference is consistent with the different optical paths of the two channels. The 1651-nm channel uses a ~1.5-km path over a wooded area, whereas the 3291-nm channel uses a shorter ~0.2-km path across the parking lot of our building, and we expect it to agree better with the in situ measurement.

The CO_2 diurnal variation is likely to arise from photosynthesis/respiration of vegetation. The larger fast fluctuation observed in the CO_2 channel is likely a result of the residual optical interference effects (etalon fringes). The H_2O channel (OPA system 2, far target) shows good agreement with in situ data, especially when there is no local emission, for example, from air-conditioning activity. The H_2O variation was relatively small in this data, since weather (pressure and temperature) was stable during the measurement.

The CO diurnal variation measured by the 4764-nm channel (OPA system 3, near target) was the largest among the four measured species. This variation is most likely a result of car traffic activity. While this kind of dynamic CO variation was previously observed in early long-path measurements using a tunable diode laser,[21] to the best of our knowledge, our measurement is the first CO open-path measurement based on OPA.

4.2 *Airborne Demonstration*

We upgraded OPA system 2 and successfully performed an airborne measurement of CH_4 at 1650.9 nm from an 11-km altitude. A NIR photo-multiplier detected a strong return signal from the earth surface from a few km in altitude. The optics components were mounted on stable, spring-free mounts, and the fiber-coupled beam expander was replaced by a free-space transmitter. Instead of the continuous-seed wavelength scan described in this paper, we implemented a stepped scan, which samples 20 wavelength points across the 1650.9-nm CH_4 line, pulse by pulse. These results will be reported in a separate paper. The successful flight demonstration confirmed that the OPA approach should enable IPDA measurements from orbit once the laser power is scaled up.

4.3 *Power Scaling for Space Implementation*

Because our system is less sensitive to alignment, it can be implemented by naturally enhancing existing Nd:YAG space laser instruments. For satellite-based instruments at altitudes of a few 100s of km, our ~10-μJ output energy has to be scaled up by a factor of $20 \sim 50$. In the experiment presented here, our output energy is limited by the pump energy (~60 μJ). If the averaged optical power densities are maintained within the crystal by using larger beam sizes, this OPA approach should be linearly scalable to a higher output power by using higher pump/seed powers without damaging the crystal. Therefore, we are looking into injection-seeded NPROs and burst-mode Yb fiber amplifiers as ways to boost the pump energy to the >1-mJ level. We have used a 600-μJ injection-seeded NPRO and have obtained a ~100-μJ signal output. The use of a fiber laser in burst mode is a new concept for OPA power scaling, and it potentially offers higher

wall-plug efficiency for space applications. We anticipate that a ~ Watt level (peak) power is needed for the seed laser. We are looking into Erbium-doped fiber amplifiers (in the 1.5-μm range) and OPAs to amplify other seed wavelengths.

In these high-pump-energy situations, spectral broadening due to back conversion may obscure detailed spectral features of low-pressure atmospheres. For example, the Doppler width of a CH_4 line at 3270.4 nm is ~240 MHz for the Martian atmosphere (~5 Torr at the surface). Although the impact due to the broadened linewidth can be largely mitigated by data analysis, keeping the laser linewidth as narrow as possible is highly desirable. Therefore, we might need to make our OPA a multiple-stage device and amplify a signal and/or an idler separately,[22] especially for Mars applications, by using a longer pump pulse (~10 ns) and larger beam size inside the crystal.

5 Conclusions

Lidar will be a key technology for the measurement of atmospheric gases with high sensitivity and resolution on global scales, and it will enhance our understanding of the current state of planetary atmospheres and geology. We have demonstrated the ability to detect diurnal variations of several atmospheric trace gases in both the NIR and MIR regimes, using OPA and cooperative hard targets. Comparative measurements of the CH_4, CO_2, and H_2O variations measured by the OPA systems and by an in situ instrument showed good agreement. We measured four important greenhouse gases using the OPA for Earth applications. Given a sufficient tuning range of the OPA, the measurements can be extended to other molecules. We believe that our approach will become a core technology in future planetary lidar instruments.

Acknowledgments

This work is supported by the NASA Astrobiology Program's Astrobiology Science and Technology Instrument Development (ASTID) Program.

References

1. National Research Council, "Earth science and applications from space: national imperatives for the next decade and beyond," http://www.nap.edu (2007).
2. G. L. Villanueva, M. J. Mumma, and R. E. Novak, "Strong release of methane on Mars: evidence of biology or geology?" in *19th Annual VM Goldschmidt Conference*, Vol. 73, p. A1384, Geochim Cosmochim Acta, Davos, Switzerland (2009).
3. Y. Chen et al., "MW+ peak power sub-nsec 10-kHz repetition rate polarization-maintaining fiber-amplifiers using tapered Yb-doped fibers," *Proc. SPIE* **8237**, 82371T (2012), http://dx.doi.org/10.1117/12.909779.
4. D.-W. Chen et al., "Narrowband Er:YAG nonplanar ring oscillator at 1645 nm," *Opt. Lett.* **36**(7), 1197–1199 (2011), http://dx.doi.org/10.1364/OL.36.001197.
5. R. A. Baumgartner and R. L. Byer, "Continuously tunable IR lidar with applications to remote measurements of SO_2 and CH_4," *Appl. Opt.* **17**(22), 3555–3561 (1978), http://dx.doi.org/10.1364/AO.17.003555.
6. M. J. T. Milton et al., "Injection-seeded optical parametric oscillator for range-resolved DIAL measurements of atmospheric methane," *Opt. Comm.* **142**(1–3), 153–160 (1997), http://dx.doi.org/10.1016/S0030-4018(97)00260-5.
7. M. Imaki and T. Kobayashi, "Infrared frequency upconverter for high-sensitivity imaging of gas plumes," *Opt. Lett.* **32**(13), 1923–1925 (2007), http://dx.doi.org/10.1364/OL.32.001923.
8. A. Amediek et al., "Development of an OPO system at 1.57 μm for integrated path DIAL measurement of atmospheric carbon dioxide," *Appl. Phys. B* **92**(2), 295–302 (2008), http://dx.doi.org/10.1007/s00340-008-3075-6.
9. D. Sakaizawa et al., "Development of a 1.6 μm differential absorption lidar with a quasi-phase-matching optical parametric oscillator and photon-counting detector for the

vertical CO_2 profile," *Appl. Opt.* **48**(4), 748–757 (2009), http://dx.doi.org/10.1364/AO.48.000748.
10. A. Fix et al., "Optical parametric oscillators and amplifiers for airborne and spaceborne active remote sensing of CO_2 and CH_4," *Proc. SPIE* **8182**, 818206 (2011), http://dx.doi.org/10.1117/12.898412.
11. A. W. Yu et al., "Mid-infrared OPO for high resolution measurements of trace gases in the Mars atmosphere," in *Laser Applications to Chemical, Security and Environmental Analysis (LACSEA)*, St. Petersburg, Florida, OSA Technical Digest (CD) (Optical Society of America), paper LMC5 (2008), http://www.opticsinfobase.org/abstract.cfm?uri=LACSEA-2008-LMC5.
12. J. Zayhowski, "Periodically poled lithium niobate optical parametric amplifiers pumped by high-power passively Q-switched microchip lasers," *Opt. Lett.* **22**(3), 169–171 (1997), http://dx.doi.org/10.1364/OL.22.000169.
13. K. Aniolek et al., "Microlaser-pumped periodically poled lithium niobate optical parametric generator-optical parametric amplifier," *Opt. Lett.* **25**(8), 557–559 (2000), http://dx.doi.org/10.1364/OL.25.000557.
14. T. J. Kulp et al., "The application of quasi-phase-matched parametric light sources to practical infrared chemical sensing systems," *Appl. Phys. B* **75**(2–3), 317–327 (2002), http://dx.doi.org/10.1007/s00340-002-0978-5.
15. T. A. Reichardt et al., "Frequency-locked, injection-seeded, pulsed narrowband optical parametric generator," *Appl. Opt.* **42**(18), 3564–3569 (2003), http://dx.doi.org/10.1364/AO.42.003564.
16. U. Bäder et al., "Pulsed nanosecond optical parametric generator based on periodically poled lithium niobate," *Opt. Comm.* **217**(1–6), 375–380 (2003), http://dx.doi.org/10.1016/S0030-4018(02)02342-8.
17. G. Ehret et al., "Space-borne remote sensing of CO_2, CH_4, and N_2O by integrated path differential absorption lidar: a sensitivity analysis," *Appl. Phys. B* **90**(3–4), 593–608 (2008), http://dx.doi.org/10.1007/s00340-007-2892-3.
18. I. T. Sorokina and K. L. Vodopyanov, Eds., *Solid-State Mid-Infrared Laser Sources*, Springer, New York (2003), ISBN 3540006214.
19. E. E. Whiting, "An empirical approximation to the Voigt profile," *J. Quant. Spectrosc. Radiat. Transfer* **8**(6), 1379–1384 (1968), http://dx.doi.org/10.1016/0022-4073(68)90081-2.
20. L. S. Rothman et al., "The HITRAN 2008 molecular spectroscopic database," *J. Quant. Spectrosc. Radiat. Transfer* **110**(9–10), 533–572 (2009), http://dx.doi.org/10.1016/j.jqsrt.2009.02.013.
21. R. T. Ku, E. D. Hinkley, and J. O. Sample, "Long-path monitoring of atmospheric carbon monoxide with a tunable diode laser system," *Appl. Opt.* **14**(4), 854–861 (1975), http://dx.doi.org/10.1364/AO.14.000854.
22. J. Burris and D. Richter, "Tunable infrared radiation for atmospheric profiling," *J. Appl. Remote Sens.* **2**, 023527 (2008), http://dx.doi.org/10.1117/1.2960975.

Biographies and photographs of the authors not available.